Preliminary Insights into Electro-Sensitive Ecolubricants: A Comparative Analysis Based on Nanocelluloses and Nanosilicates in Castor Oil

Moisés García-Morales [1],* , Samuel D. Fernández-Silva [1], Claudia Roman [1], Marius A. Olariu [2], Maria T. Cidade [3] and Miguel A. Delgado [1]

[1]   Departamento de Ingeniería Química, Centro de Investigación en Tecnología de Productos y Procesos Químicos (Pro2TecS), Campus de "El Carmen", Universidad de Huelva, 21071 Huelva, Spain; samuel.fernandez@diq.uhu.es (S.D.F.-S.); claudia.roman@diq.uhu.es (C.R.); miguel.delgado@diq.uhu.es (M.A.D.)

[2]   Department of Electrical Measurements and Materials, Faculty of Electrical Engineering, Bd. Prof. Dimitrie Mangeron 53, "Gheorghe Asachi" Technical University of Iasi, 700050 Iasi, Romania; olarium2003@gmail.com

[3]   Departamento de Ciência dos Materiais, CENIMAT/I3N, Faculdade de Ciências e Tecnologia, Universidade Nova de Lisboa, 2829-516 Caparica, Portugal; mtc@fct.unl.pt

*   Correspondence: moises.garcia@diq.uhu.es; Tel.: +34-959-218207

check for updates

Abstract: The newest generation of lubricants needs to adapt to stricter environmental policies. Simple and sustainable formulations with tunable rheological properties under the action of electric potentials may be the key. The present research explored the feasibility of producing electro-sensitive ecolubricants based on nanocellulose (crystalline and fibrillar) or nanoclay (Cloisite 15A montmorillonite and halloysite nanotubes) dispersions in castor oil, at concentrations that ranged from 2 to 6 wt.%. Broadband dielectric spectroscopy (BDS) measurements allowed for a first estimate on the electro-responsive potential of the nanofluids. The nanocelluloses and the montmorillonite suspensions presented a relaxation event in the dielectric loss, ε'', centered at ca. 2–4 kHz, which is related to interfacial polarization. Moreover, their actual electro-rheological (ER) effect under high electric potentials up to 4 kV/mm was assessed by determining the magnitude of the yield stress from steady flow curves at 25 °C. It was found that the nanocelluloses and the montmorillonite showed an enhancement of three orders of magnitude in their yield stress values at 4 kV/m. This enhancement was much greater than in the halloysite nanoclay, which did not exhibit any polarization). This is the starting point for the development of environmentally friendly ER lubricating fluids, based on nanocellulose and montmorillonites (layered nanosilicates), which might assist in reducing the friction and wear through the application of controlled electric fields.

Keywords: ecolubricants; nanocellulose; nanoclays; castor oil; electro-rheology; dielectric spectroscopy; smarts fluids; nanofluids

1. Introduction

Over the last few decades, the extensive research carried out on lubricating fluids has enabled more efficient formulations. However, this noticeable improvement in their tribological properties has arisen at the expense of the use of chemicals which may represent potential health risks for the population. In fact, about 50% of waste lubricants worldwide is estimated to end up in the environment, thus contributing substantially towards the degradation of critical resources, mainly water [1].

The above concern on the development of environmentally respectful lubricants has encouraged the search of alternatives. Thus, remarkable advances can be found around the formulation of blends of vegetable oil and non-toxic polymers, such as recycled polypropylene or the ethylene and vinyl acetate copolymer [2], celluloses and cellulosic derivatives [3,4] or chitin and chitosan [5], to name a few. There has also been a growing interest in the use of "nanolubricants", i.e., nanoparticles with remarkable friction-reducing and anti-wear properties, for replacing the hazardous additives currently used in lubricants [6]. Among the nanoparticles with proven tribological performance are carbon nanotubes, carbon onions, nanodiamonds, graphene, BN/ZrO2/TiO2 nanoparticles or the Inorganic Fullerene-like (IF) metal disulfides (IF-MoS2, IF-WS2) nanoparticles, for which a variety of mechanisms have been proposed to explain the lubrication enhancement according to their size, structure and morphology [7]. Even so, some of these nanoparticles may still induce toxicological effects. Attempts on the use of different types of harmless nanoparticles in the development of "greener" lubricants can be also found. For example, Zhang et al. [8] reported the use of nano cellulose fatty acid esters in paraffin oil, whilst Martin-Alfonso et al. [9] studied the rheological and tribological behavior of eco-friendly lubricating greases where sepiolite nanoclay was utilized as a gelling additive in castor oil [9]. Despite the benefits proven by those studies, such formulations may present limitations in terms of accommodating optimally varying local lubrication regimes, including high- and low-temperature effects on viscosity [10].

In that sense, a successful performance over a wide range of in-service temperatures and at different lubrication regimes can probably be only achieved through lubricants whose properties can be tuned under the application of external stimuli like an electric field, i.e., "smart" lubricants. Electro-rheological (ER) fluids are materials that switch from liquid-like to solid-like upon application of an electric field [11]. The main group of ER fluids is that constituted by dispersions of polarizable particles in a non-conductive carrier, typically an oil. Liquid crystals (LC) is the second group. However, LCs do not present potential utility as industrial lubricants (they might need to sustain high temperatures) unless they include chemicals which may cause harm to the environment [12,13]. Regarding the main group, the electric field induces attractive interactions between the suspended particles that enable them to rapidly form a solid-like network of chain (and/or column)-like structures perpendicular to the parallel electrodes [14,15]. ER materials cover a wide variety of particles with sizes in the nanometer to micrometer scale and various shapes including spherical and non-spherical [15].

With a view to obtaining 100% environmentally friendly lubricants, nanocellulose and nanoclays are of special interest because of their harmless character, abundant availability and wide range of aspect ratios which can entail varying tribological mechanisms. Moreover, castor oil is a good candidate as dispersing medium due to its good lubricity and high viscosity. Cellulose nanocrystals (CNC) and cellulose nanofibrils (CNF) are nanoscale cellulose fibers with different shape and size which have shown reinforcing effects in polymer nanocomposites. Even though cellulose (and its derivatives) dispersions in oil have revealed very noticeable electro-responsive capacity [16], little emphasis has been placed on the ER behavior of nanocellulose dispersions, and in no case was lubrication among the applications described. CNCs are needle-like cellulose crystals of 10−20 nm in width and several hundred nanometers in length, while CNFs form long flexible fiber networks with a fibril diameter similar to or larger than CNCs [17]. With regards to the nanoclays, their varying structures allows for the evaluation of shape and size effects while maintaining, in the case of natural clays, a great similarity in chemical composition [18]. Montmorillonite is a type of layered nanosilicate (also called phyllosilicate), belonging to the smectite group, constituted by two tetrahedral sheets of silica sandwiching a central octahedral sheet of alumina (platelets). Negative charges at the interlayer galleries are counterbalanced by positive ions (Na^+ mainly) which bind the platelets together. Halloysite-(10 Å), also a phyllosilicate nanoclay, is a dioctahedral hydrated polymorph of kaolinite with a monolayer of water molecules between the 1:1 aluminosilicate layers which naturally occurs in the form of nanotubes. Halloysite-(10 Å) can irreversibly dehydrate to halloysite-(7 Å) [19].

So far, very few studies have explored the potential interest of the electro-rheological phenomenon in relation with the development of electro-sensitive lubricants [13,20]. In the scarce existing literature, a reduction in the friction coefficient was attributed to the electro-viscous effect as a consequence of the alignment of a particulate phase [10] or a nematic phase in the case of LCs [12,13] under the electric field applied. In fact, the mixed boundary lubrication regime occurs when the two sliding surfaces are not fully separated by the fluid film and some contact of asperities occurs. In this regime, the smart lubricant viscosity will be increased, by the action of the electric field, to reduce the coefficient of friction and wear [10]. Moreover, the electric field would contribute to lure the electro-sensitive nanoparticles from the outer parts of the bearing into the contact point, thereby mitigating the effects provoked by the direct contact between the sliding surfaces. According to Ikazaki et al. [21], interfacial polarization (also called "Maxwell-Wagner" polarization) is basically responsible for the ER effect. In fact, the magnitude of the polarization is thought to determine the magnitude of the ER effect. Moreover, the competition between the polarization, that tends to align the chains with it, and the flow field, that tends to destroy the chains determines whether or not the chain-like structure is maintained under the flow conditions.

Based on the above ideas, it is necessary to evaluate the electro-viscous potential of the nanocellulose- or nanoclay-castor oil dispersions before it can be definitely stated that they are promising candidates to catalyze a "new generation" of ecolubricants based on the application of an external electric field. On these grounds, we report preliminary results on the dielectric properties and electro-rheological behavior of lubricating fluids made up of cellulose nanocrystals/nanofibrils or clay mineral (Cloisite 15A montmorillonite and halloysite nanotubes) nanoparticles in castor oil, at concentrations that ranged from 2 to 6 wt.%. The development of sustainable lubricants has never been approached in this manner, to the best of our knowledge, thus representing cutting-edge research on reduction of friction and wear.

2. Materials and Methods

2.1. Materials

Commercial cellulose nanocrystal (CNC) with 10–20 nm diameter and 0.3–0.9 m length, and cellulose nanofibril (CNF) with 10–20 nm diameter, 2–3 m length and crystallinity (measured by X-ray Diffraction, XRD) of 92%, were purchased from NANOGRAFI Co. Ltd. (NANOGRAFI Co. Ltd., Jena, Thuringen, Germany). Regarding the nanoclays, Cloisite 15A and halloysite nanoclay were chosen as representatives of planar and tubular layered nanosilicate, respectively. Cloisite 15A, a montmorillonite modified with dimethyl dihydrogenated-tallow quaternary ammonium chloride (hydrogenated-tallow with composition ~65% C18, ~30% C16 and ~5% C14), was provided by Southern Clay Products (Southern Clay Products, Austin, TX, USA). This clay (90 vol% of its particles are smaller than 13 m) presents a cation exchange capacity of 125 meq/100g clay and interlayer distance d_{001} (XRD) of 31.5 Å. Halloysite nanoclay, a natural layered aluminosilicate in the form of nanotubes, with 30–70 nm diameter and 1–3 m length, and with a cation exchange capacity of 8 meq/g clay, was supplied by Sigma Aldrich (Sigma Aldrich, St. Louis, MO, USA). Castor oil was purchased from Guinama (Guinama, Valencia, Spain). Physicochemical properties of this vegetable oil can be found elsewhere [22]. The chemical treatment with surfactant on the Cloisite 15A particles improved their dispersibility in castor oil, thus yielding more stable dispersions as compared to the natural Halloysite nanotubes.

2.2. Nanofluids Processing

"As-received" nanocellulose and nanoclay were used in the preparation of the nanofluids, at concentrations of 2, 4 and 6 wt.%, according to a two-step protocol as reported by Maheswaran and Sunil [23]. First, the corresponding quantity of the nanoparticle was pre-dispersed in 25 g approx. castor oil in small glass vessels by using a small magnetic stirrer, at 50 °C and for 45 min. Subsequently, the samples were sonicated in a Power Sonic 405 sonication bath (Hwashin Technology Co., Seoul,

Korea) at its maximum power, also at 50 °C and for 45 min. In all cases, visual inspection allowed concluding that the dispersion quality was good.

2.3. Nanofluids Characterization

The polarizability of the dispersions of nanoparticles in castor oil was assessed by broadband dielectric spectroscopy (BDS) measurements carried out at 25 °C with a Broadband Dielectric Spectrometer Alpha-A High Performance Frequency Analyzer (Novocontrol Technologies GmbH & Co. KG, Montabaur, Germany), at 1 V, in an alternating current (AC) frequency window between 1 Hz and 200 kHz. The liquid was confined in a special cell consisting of two brass electrodes with a 0.5 mm thick Teflon spacer in between. These tests allowed for a first estimate on the electro-rheological potential of the nanofluids on a fast-track basis.

Subsequently, steady-state viscous flow curves at 25 °C were performed at increasing values of the DC electric field up to 4 kV/mm, in a shear rate interval from 0.1 to 100 s^{-1}. The strain-controlled ARES G2 rheometer (TA Instruments, New Castle, DE, USA), equipped with a special electro-rheocell, a Keysight 33210A (Agilent Technologies Inc., Santa Clara, CA, USA) electric field generator and a Trek 609E-6 high-voltage power amplifier (Trek Inc., Lockport, NY, USA), was used. A plate-plate geometry with 25 mm diameter and 0.5 mm measuring gap was selected. In such a way, it was possible to evaluate the actual electro-rheological performance of the nanofluids based on the yield stress values arisen, at the lowest shear rates imposed, under the action of electric fields. It was also possible to measure the current intensities through the fluid and so to calculate the corresponding leak current densities.

All these tests were carried out, at least, three times for every sample, and data shown have statistically significant values, i.e., they did not exceed a significance level of 0.05 in Student's t-tests and had a 95% confidence interval.

3. Results and Discussion

3.1. Preliminary Evaluation of the Nanofluids' Electro-Sensitive Potential by Dielectric Characterization

In case of suspensions, interfacial polarization (also called "Maxwell-Wagner" polarization), provoked by the electric field and due to the difference in dielectric constant between the particles and the dispersing medium [24], is known to be the main responsible for the electro-rheological phenomenon [25]. Thus, broadband dielectric spectroscopy (BDS) measurements may shed light on their ER potential. The neat castor oil has also been included as a reference. The polarization rate is the most important factor in generating a high ER effect. It is quantified by the frequency at which the dielectric relaxation occurs. Only relaxations within the frequency window between 100 Hz and 100 kHz produce a significant ER effect [21]. The relaxation frequency is defined as a local maximum of the dielectric loss, ε'.

Figure 1 presents the evolution of the dielectric constant, ε', and dielectric loss, ε', with AC frequency in the interval from 1 Hz to 200 kHz for the CNC and CNF dispersions. As displayed in Figure 1b, the interfacial polarization of cellulose nanocrystals and cellulose nanofibrils at 2 wt.% is evidenced by a broad relaxation event, centered at ca. 2–4 kHz, that extents over three decades of frequency (10^2 to 10^5 Hz). For the sake of clarity, the data corresponding to these two 2 wt.% dispersions are plotted with *Y*-axis in linear scale in an inset. The broadness of the ε'-peak is caused by overlapping peaks due to the different orientations of the nanocellulose particles in suspension [26]. This result might be a consequence of nanocrystals and nanofibrils with varying diameters and lengths. With increasing the concentration, such a relaxation event becomes less defined and approaches a limiting curve.

Moreover, the extent of the polarization can be assessed by the difference between the dielectric constant values at both sides of the frequency at which the relaxation peak appears, i.e., $\Delta\varepsilon' = \varepsilon_0' - \Delta\varepsilon_\infty'$. Thus, under comparable relaxation frequencies, the higher the $\Delta\varepsilon'$, the more remarkable the

ER effect will be [15]. Values of 10 Hz and 200 kHz were chosen as low and high frequencies, f_0 and f_∞, respectively. As expected, a decrease in ε' was observed with increasing frequency in Figure 1a. A noticeable increase in ε' was observed at the lowest frequencies when the nanocellulose was added to castor oil, in varying concentrations. Higher nanocellulose concentrations yielded larger values of ε'. Moreover, despite their different aspect ratio, the observed behavior did not seem to be, in general, too sensitive to the type of cellulose. This result is probably a consequence of both CNC and CNF showing fiber-like shape and having similar chemical composition.
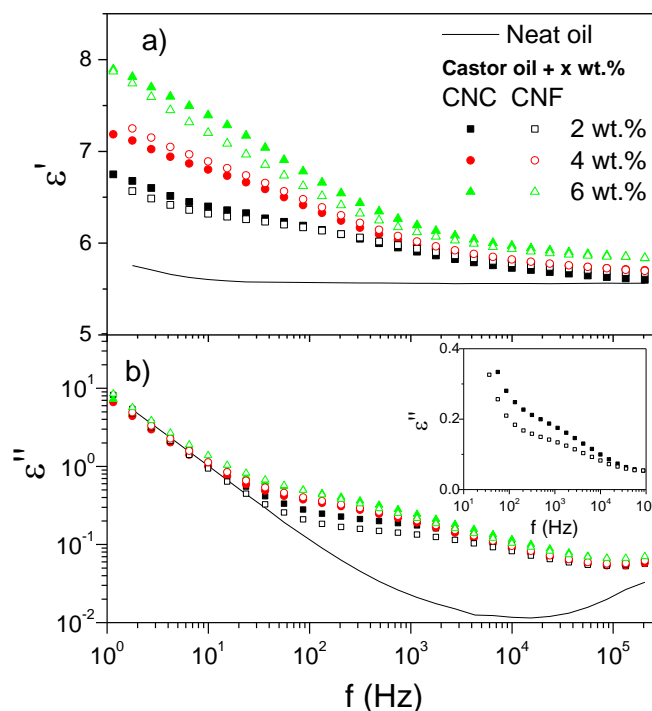
Figure 1. Frequency dependence of (**a**) the dielectric constant, ε', and (**b**) the dielectric loss, ε'', at 25 °C for cellulose nanocrystals and cellulose nanofibrils dispersions in castor oil, as a function of cellulose concentration. (Inset: 2 wt.% dispersions with *Y*-axis in linear scale).

Conversely, the two selected nanoclays demonstrated completely different dielectric behaviors. In this case, not only was their shape but also their chemical composition quite distinct. Cloisite 15A is composed of platelets, and the sodium ions into its clay galleries have been replaced with dimethyl dihydrogenated-tallow quaternary ammonium ions, thereby altering its dielectric properties (and also lipophilicity) as compared to a natural hydrophilic montmorillonite clay mineral. Halloysite naturally occurs in the form of nanotubes, and has not been chemically treated with any surfactant. Regarding Cloisite 15A, Figure 2b also provides clear evidence on the existence of interfacial polarization as proven by a relaxation shoulder which extends over a smaller frequency range as compared to the nanocelluloses above. However, this shoulder has been partially masked (less defined than in the nanocelluloses) by the contribution of a higher AC conductivity, as demonstrated by the high values of ε'' corresponding to the low frequency region [26]. Moreover, there also seems to be a limiting dielectric loss behavior with increasing the nanoclay concentration. With regards to the dielectric constant, the enhancement in the ε_0' values provoked by an increase in the concentration is very remarkable (Figure 2a). A plateau region appears at the lowest frequencies in the ε' curves. The halloysite nanotubes, in contrast, did not show any relaxation peak in the frequency range of interest (Figure 2b). Moreover, the measured values of ε' were very small as compared to the other nanoparticles studied, thus demonstrating poor polarization capacity.
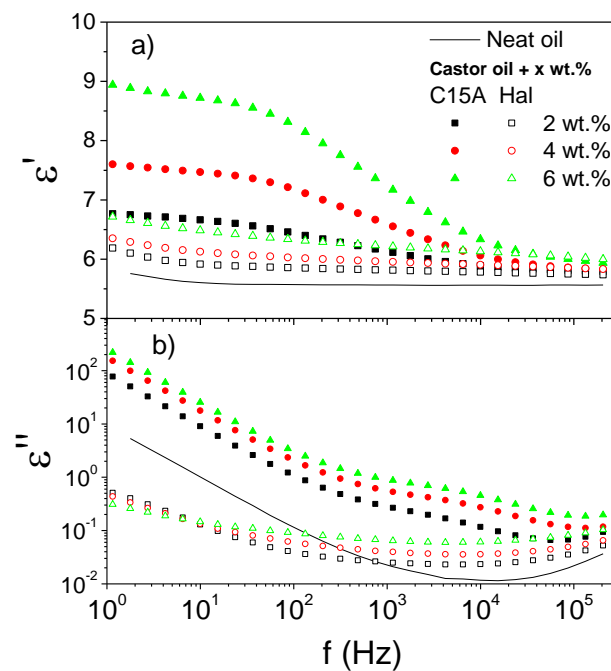
Figure 2. Frequency dependence of (**a**) the dielectric constant, ε', and (**b**) the dielectric loss, ε'', at 25 °C for Cloisite 15A and halloysite dispersions in castor oil, as a function of nanoclay concentration.

Figure 3 depicts the evolution of the dielectric constant (also referred to as permittivity) drop, $\varepsilon' = \varepsilon'_{10Hz} - \varepsilon'_{200kHz}$, with nanoparticle concentration, at 25 °C. Three different behaviors are observed. Both Cloisite 15A and halloysite nanotubes presented a linear dependency of $\Delta\varepsilon'$ with concentration. However, in the latter case, the $\Delta\varepsilon'$ values measured were so small that the nanotubes are not expected "a priori" to exhibit an important ER effect. Moreover, they did not show the relaxation event which characterizes the interfacial polarization mechanism. In contrast, Cloisite 15A is expected to be highly electro-responsive and to present a very good ER capacity, given the strong interactions that should arise from highly polarized particles. This behavior would be enhanced with increasing the nanoclay concentration. As for the nanocelluloses (an overall trend line is provided), Figure 3 displays, in general, a first marked increase in $\Delta\varepsilon'$ at 2 wt.% followed by a smoother evolution at higher concentrations. An intermediate level of ER performance would be then expected, according to these results.
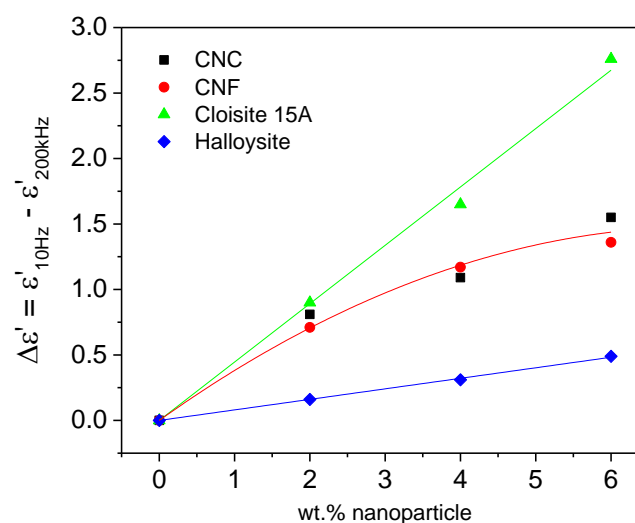

Figure 3. Evolution of the dielectric constant (permittivity) drop, $\Delta\varepsilon' = \varepsilon'_{10Hz} - \varepsilon'_{200kHz}$, with nanoparticle concentration at 25 °C.

As previously described, the relaxation event corresponding to the interfacial polarization of Cloisite 15A in castor oil was partially masked by a higher electrical conductivity when the oil was filled with this type of nanoparticle. In that sense, at any of the three concentrations studied, a low frequency AC conductivity plateau is observed in Figure 4b, suggesting the formation of conductive structures between the electrodes, at an electric potential as low as 1 V (used in the dielectric spectroscopy tests). It is worth mentioning that the value of the AC conductivity plateau is, in actuality, the direct current (DC) conductivity [27]. Furthermore, the AC conductivity plateau value was seen to increase with concentration. Nevertheless, the castor oil's AC conductivity did not vary upon the addition of the nanocelluloses (Figure 4a), whilst the halloysite nanotubes brought about, at the lower bound of the frequency interval studied, a reduction in the AC conductivity as compared to the neat oil (also shown by the ε'' curve in Figure 2b). These results allow drawing two interesting conclusions. First, at concentrations equal to or higher than 2 wt.%, the Cloisite 15A montmorillonite forms electrical percolated structures in castor oil, thereby enhancing the ER effect. Moreover, lower leak current density values during the ER tests are expected for the halloysite nanotubes and the nanocelluloses, as will be demonstrated below.
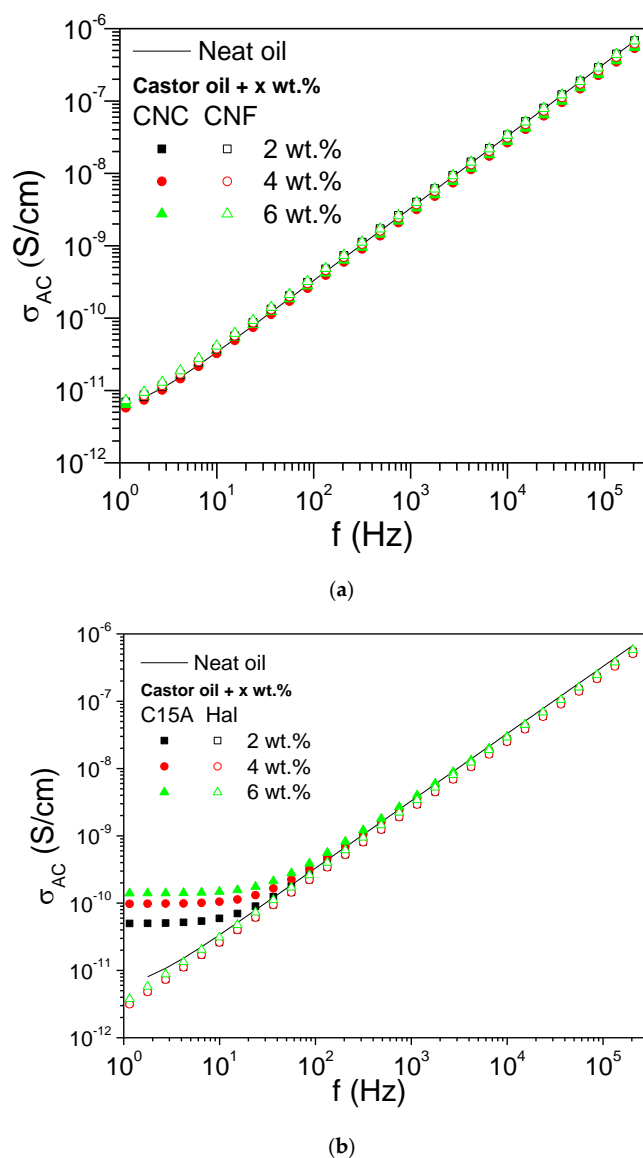

(a)

(b)

Figure 4. Frequency dependence of the AC conductivity, σ_{AC}, at 25 °C for (**a**) the nanocelluloses and (**b**) the nanoclays dispersions in castor oil, as a function of their concentration.

3.2. Electro-Rheological Flow Behavior of the Nanofluids

Further to this preliminary dielectric characterization, the actual electro-rheological potential of the above nanofluids was studied by means of steady state viscous flow curves at 25 °C. The shear rate sweep is a commonly used method of measuring the stability of the formed particle structures [15]. As Seo et al., [14,28] pointed out, the viscous flow behavior of ER fluids can be described using different rheological models. Regarding the nanocellulose fluids, their ER behavior is exemplified in Figure 5 with a selected concentration of 4 wt.%. At electric field strengths equal to or higher than 0.080 kV/mm the dispersions behaved like "plastic" fluids, characterized by an electric field dependent yield stress value at the lowest shear rates, followed by a Newtonian evolution of the shear stress (τ) with the shear rate ($\dot{\gamma}$). The test in the absence of electric potential has been included for reference, showing a straight line with slope of 1 in log-log scale, thus confirming the Newtonian character of the fluids when E = 0 kV/mm. Slight deviations observed at the lowest shear rates are a consequence of technical limitations (lack of sensitivity). However, at lower E values, the stresses decreased with shear rate and passed through a minimum before approaching the final Newtonian behavior. Under low electric fields, the formed structures can be broken by the action of high enough hydrodynamic forces (shear stresses). The "healing" effect provoked by the electric field that tend to realign the particles was not sufficient to re-establish the initial structure. Thus, the stresses decreased with the shear rate up to a critical value when the structures fully broke and the dispersions showed a complete liquid-like behavior [28]. Such an overall behavior can be described over a wide range of shear rates by the Cho–Choi–Jhon (CCJ) empirical model (six parameters):

$$\tau = \frac{\tau_y}{1 + \left(t_1 \cdot \dot{\gamma}\right)^\alpha} + \eta_\infty \cdot \left[1 + \frac{1}{\left(t_2 \cdot \dot{\gamma}\right)^\beta}\right] \cdot \dot{\gamma} \tag{1}$$

where τ_y is the so-called "static" yield stress, η_∞ is the high-shear-limiting viscosity, t_1 and t_2 are time constants, and α and β are related to the minimum in the shear stress [14]. It is noteworthy that such a "static" yield stress differs from the dynamic yield stress which is associated to simpler models (e.g., Bingham model) and which is calculated simply by extrapolating the $\tau(\dot{\gamma})$ curve back to the shear stress intercept at a shear rate of zero. The "static" yield stress is the shear stress required to initiate shear flow in a fluid initially at rest, thus being higher that the dynamic yield stress in fluids which present a minimum stress like the nanocellulose-based fluids shown in Figure 5 [14]. As an example, and in order to promote further discussion on the effect of the above parameters, the best-fit values corresponding to the CCJ model parameters at every electric field strength tested are gathered in Table 1 for the CNF fluid at 4 wt.% (Figure 5b). It can be observed that the minimum stress values in Figure 5b are smaller than the stress values displayed in Table 1, thereby confirming that the parameter τ_y is actually a "static" yield stress. Moreover, t_1 and t_2 (time constants) are the inverse critical shear rates at which the first and second terms, respectively, that compose Equation (1) dramatically change their slope, and so they are associated to the onset on the minimum stress peak. Hence, in general, both t_1 and t_2 are seen to decrease with increasing the electric field strength. The high-shear-limiting viscosity remains the same, 0.872 Pa·s, no matter the value of E. Finally, α also decreases as the electric field strength is raised because the peak becomes less remarkable, whilst β always remains at the upper limit of the feasible interval, between 0 and 1, because $d\tau/d\dot{\gamma} \geq 0$ [14].

The critical shear rates at the minimum stress shifted to higher values with increasing the electric field strength, because higher hydrodynamic forces are needed to destroy the electrostatic interactions. From an electric field strength of 0.8 kV/mm, no minimum stress was observed, because the electrostatic interactions were large enough so as to maintain the structure unaltered until it eventually broke and the Newtonian flow behavior commenced. The ER potential of the cellulose nanoparticles in castor oil was corroborated not only by a remarkable increase, of more than three orders of magnitude, in the shear stress with the electric field, but also by the fact that the solid-like behavior extended up to shear rates values as high as 100 s^{-1} when the electric field applied is equal to or higher than 1.60 kV/mm.
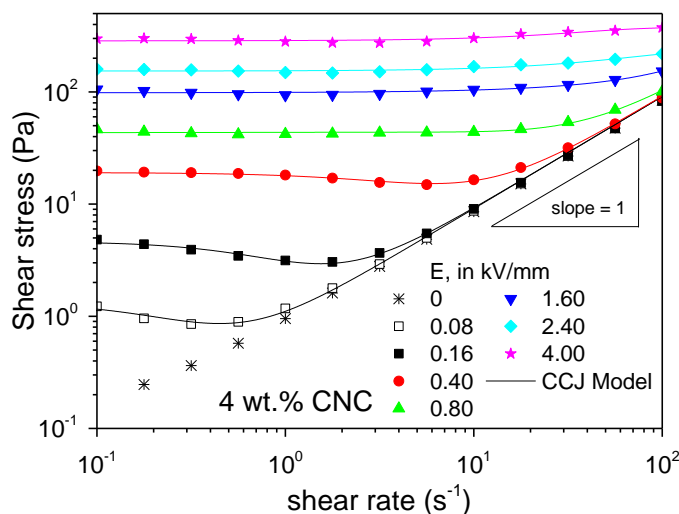
(**a**)
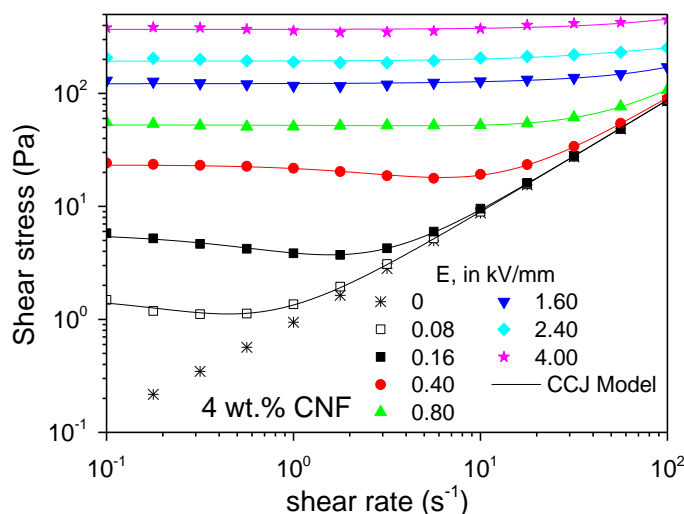
(**b**)

Figure 5. Steady state flow curves at 25 °C for 4 wt.% dispersions of (**a**) cellulose nanocrystals, CNC, and (**b**) cellulose nanofibrils, CNF, in castor oil, as a function of electric field strength.

Table 1. Fitting parameters of Equation (1) for the 4 wt.% cellulose nanofibrils (CNF) dispersion in castor oil, at the different electric field strengths tested.

| CCJ Parameters	Electric Field Strength (kV/mm)						
	0.08	0.16	0.40	0.80	1.60	2.40	4.00
τ_y (Pa)	1.50	5.70	21.45	49.28	115	177	375
t_1 (s)	3.58	1.20	0.19	0.019	0.015	0.027	0.0072
t_2 (s)	3.85	2.98	0.32	0.25	0.025	0.0086	0.0051
α	1.22	1.10	1.07	0.90	0.36	0.16	0.088
β	1.00	1.00	1.00	1.00	0.98	0.96	0.96
η_∞ (Pa·s)	0.872	0.872	0.872	0.872	0.872	0.872	0.872

Flow curves, at 25 °C, at increasing electric fields up to 4 kV/mm in Figure 6a also illustrate the high electro-rheological performance of the Cloisite 15A organo-modified montmorillonite, at 4 wt.%, with an enhancement in the yield stress with the electric field of up to three orders of magnitude. Even so,

despite the previous conclusions drawn from the dielectric characterization, the yield stress achieved at the highest E of 4 kV/mm was of ca. 200 Pa, so being on the same order than that corresponding to the nanocellulose (ranging 300–400 Pa). In that sense, it is noteworthy that Cloisite 15A was much less sensitive to the lowest E than the nanocelluloses. In fact, it was not until an electric field of 0.40 kV/mm was applied that an effective yielding behavior was attained. At 0.16 kV/mm, for example, the effect was very small (Figure 6a) and so this curve was not used further in this study. The ER behavior corresponding to this layered nanosilicate can be described by a simpler model than above, i.e., the Bingham model (two parameters):

$$\tau = \tau_y + \eta_\infty \cdot \dot{\gamma} \tag{2}$$

where τ_y is the dynamic yield stress and η_∞ is the high-shear-limiting viscosity. However, the behavior observed at the highest E intensities slightly deviates from the traditional "plastic" behavior described by Equation (2). In fact, there appears to be a stress shoulder before the actual liquid-like behavior is finally attained. Moreover, the shear rate at which this shoulder is centered moved to higher values as the electric field strength was increased. Even in the absence of flow, a structure formed due to the electrostatic interaction of polarized nanoclay platelets that align parallel to the electric field [29]. Under intermediate to high shear stress conditions, the platelets released from the broken structures are orientated by the hydrodynamic forces parallel to the electrodes so that the flow resistance is reduced. At very high E values, more stable structures may have arisen due to larger interacting areas, thus causing the observed shoulder.

In contrast, the ER performance of the halloysite nanotubes was as poor as expected from the previous dielectric properties analysis. The yield stress values were much lower than in the Cloisite 15A layered nanosilicate, at comparable concentrations and electric fields. Kuznetsov et al. [30] explained such a difference by formation of more strong chain-like structures from interacted plates rather than tubes. A limiting yield stress value of ca. 10–20 Pa at 4 wt.% was found (Figure 6b). Moreover, even at the highest E intensities, the Newtonian behavior was clearly achieved at the upper range of shear rates tested, thus manifesting the less strong chain-like structures and a poor ER response. Their poor dielectric properties (no dielectric relaxation observed between 10 Hz and 100 kHz, and very small value of $\Delta\varepsilon'$) and their morphological (rod-like) characteristics, must be the reasons behind this behavior. The flow behavior in Figure 6b was also fairly well described by the CCJ empirical model in Equation (1). However, the minimum in the shear stress curve, which appeared at the highest electric field strengths, was less pronounced than in the nanocelluloses.
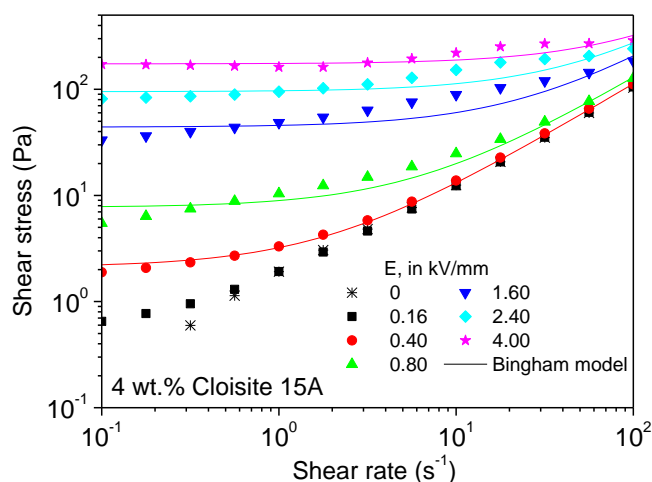
(a)

Figure 6. *Cont.*
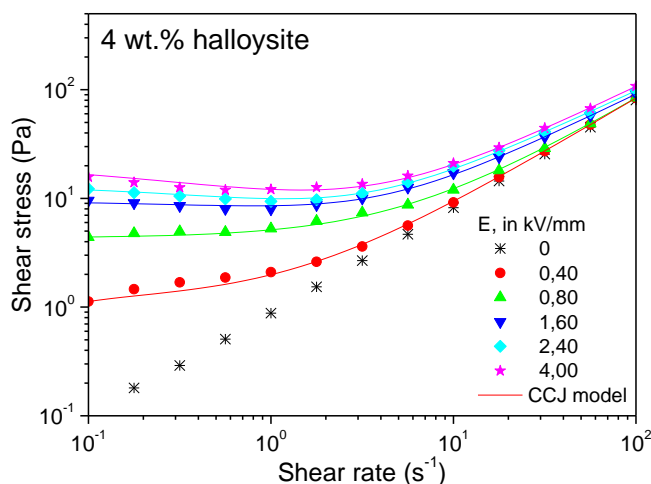
(**b**)

Figure 6. Steady state flow curves at 25 °C for 4 wt.% dispersions of (**a**) Cloisite 15A and (**b**) halloysite nanoclay in castor oil, as a function of electric field strength.

The static/dynamic yield stress values τ_y, as obtained from best fit of experimental data to Equation (1) or Equation (2), as appropriate, were plotted against the imposed electric field strength in Figure 7. For the nanocellulose dispersions at the concentrations of 4 and 6 wt.%, the evolution of τ_y with E, in the electric field range from 0.16 to 4 kV/mm, was fitted by a power-law scaling, as expressed by Equation (3):

$$\tau_y(E) = a \cdot E^b \tag{3}$$

where in Equation (3) above, a is the static/dynamic yield stress at an electric field strength of 1 unit (in this case 1 kV/mm), and b is a parameter which according to the classic polarization model should have a value of 2. However, this value very often deviates from 2, given that most of the real fluids with industrial interest often differ from being "idealized dispersions of hard dielectric spheres treated as point dipoles" [24].

Regarding the nanocelluloses, a limiting behavior was observed with increasing concentration. Moreover, differences due to cellulose type (nanocrystals or nanofibrils) were not found to be statistically significant at the 0.05 level. Thus, although a very slight deviation was appreciated at the highest electric field strengths, their overall behavior at concentrations of 4 and 6 wt.% has been described by a unique linear relationship. The "a" and "b" parameters, as obtained from linear best fit in double-log plot (Figure 7a), are gathered in Table 2.

This limiting behavior could be ascribed to the smoother evolution of $\Delta\varepsilon'$ with concentration, at weight fractions higher than 2 wt.%, previously reported in relation to Figure 3. Regarding the 2 wt.% dispersions, Equation (3) is still valid as long as it is applied, separately, at two electric field intervals delimited by a critical value, $E_c = 0.94$ kV/mm, at which both straight lines in double-log scale intercept. Thus, for E > 0.94 kV/mm, the exponent b was 0.72, whilst for E < 0.94 kV/mm, the exponent b was 1.43. Sheng and Wen [31] attributed this critical value to saturation on the interfacial polarization, thereby shifting to higher E values with increasing the nanoparticle concentration. In no case, values of the "b" exponent close to 2 were observed, due most probably to the nanocellulose nonspherical shape, mainly [24].

As shown in Figure 7b, Cloisite 15A also follows the evolution of the yield stress with the electric field described by Equation (3) in the interval from 0.4 to 4 kV/mm. At lower E values (for example, 0.16 kV/mm in Figure 6a, the ER effect was so weak that the resulting dynamic yield stress deviates from the above behavior [14,24]. Moreover, the evolution of this yielding behavior with concentration is as expected from Figure 3, i.e., a linear increase. The "b" exponents, between 1.87 and 2.00 (Table 2),

were much higher than in the nanocelluloses and were found to be very close to the universal value derived from the polarization model, i.e., b = 2. It might be that the surfactant used to replace the interlayer sodium ions in the nanoclay has enhanced the dispersion of tactoids and platelets in the oil, thus yielding a fluid exhibiting a more ideal polarization behavior [18] than that expected from nanocelluloses which tend to form fiber networks. Even so, lower values of the "a" parameter than in the nanocelluloses were observed (Table 2), most probably because the nanocelluloses were more sensitive to the application of very low electric fields, thereby affecting their overall ER behavior.
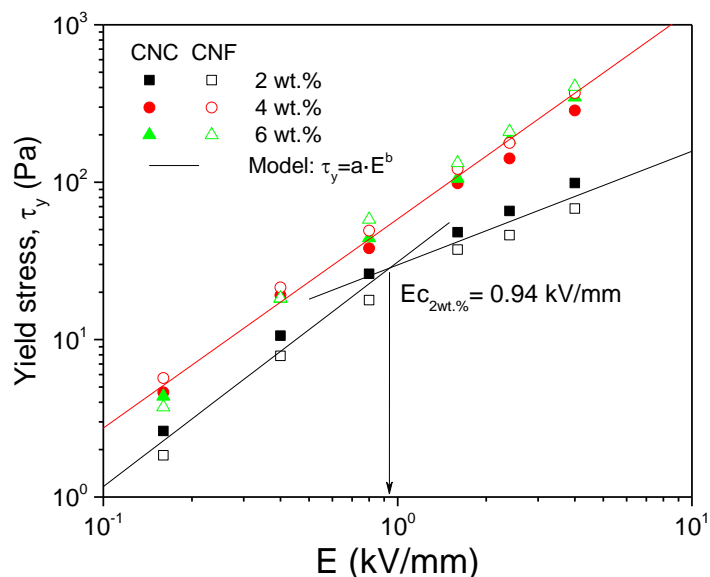
(**a**)
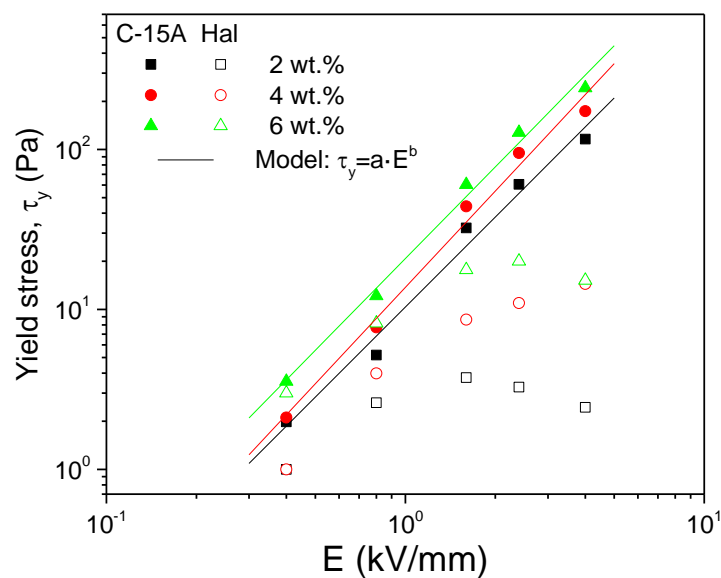
(**b**)

Figure 7. Evolution of the yield stress with the electric field strength for (**a**) the nanocelluloses and (**b**) the nanoclays dispersions in castor oil.

**Table 2.** Fitting parameters of Equation (3) for the different 2 to 6 wt.% dispersions in castor oil.

Samples	"b" in Equation (3) [unitless]	"a" in Equation (3) [Pa·(kV/mm)$^{-b}$]
Celluloses (2 wt.%)	1.43 (E < 0.94 kV/mm) 0.72 (E > 0.94 kV/mm)	31.1 (E < 0.94 kV/mm) 29.8 (E > 0.94 kV/mm)
Celluloses (4–6 wt.%)	1.33	58.4
Cloisite 15A (2 wt.%)	1.87	10.3
Cloisite 15A (4 wt.%)	2.00	13.7
Cloisite 15A (6 wt.%)	1.90	20.8

Regarding the halloysite nanotubes, they presented a clear different behavior which did not obey Equation (3). Due to their much lower ER potential, their yield stress dependence with the electric field showed a maximum yield stress value (or a limiting behavior). Kuznetsov et al. [30] reported a similar evolution for concentrations of the "as received" halloysite of 1 and 2 wt.% in silicone oil suspensions, but not at higher concentrations. However, the dielectric behavior they found was different as compared to that in Figure 2. Given their poor polarizability, the particles chains might have achieved their maximum structuring level. With time and stronger electric field strengths, a slight depletion may arise in this weak structure thereby provoking some reduction in the yield stress.

In fact, the halloysite nanoparticles randomly orientate and agglomerate under the influence of electric fields, thus yielding structures with weaker field-induced mechanical strength than the layered nanosilicates. Rozynek et al., [32], by using the wide angle x-ray scattering (WAXS) technique on clay-paraffin wax blends that were previously suggested to an electric field, concluded that kaolinite particles (layered nanosilicate) were preferentially arranged with their basal planes being parallel to the electric field direction, thus presenting a strong anisotropy. On the contrary, Halloysite/paraffin wax blends did not show any anisotropy at all, probably because their different and irregular shapes did not enable ordered structures. Moreover, Kuznetsov et al., [30] reported that interacting plates yield more strong chain-like structures than interacting tubes, due to a larger overlapping area in the former case. Based on these comments and on the results shown in Figures 5 and 6, it might be that the minima that appear in the fiber-like (nanocelluloses) and rod-like (nanotubes) particles are a consequence of the breakup of weaker structures. Therefore, a more complex model than the Bingham model, i.e., CCJ model, needs to be adopted in order to explain their rheological response. References to the use of the CCJ model for other types of fiber-based dispersions, e.g., titanium dioxide nano-whiskers, semiconducting polymer-based nanofibers, etc., can be found elsewhere [33,34]. Even so, it is possible to find such a described behavior associated to nanosheet-based fluids [25], so further insights into the issue are still required.

The above results, therefore, may have outstanding implications on the effective electro-active control of the lubrication process. Given their high polarizability and ER performance, both nanocelluloses and organomodified montmorillonite may promote an enhanced lubrication under the mixed lubrication regime, when the two surfaces are not fully separated by the fluid film and a higher-viscosity lubricant can reduce the coefficient of friction [10]. Moreover, another important aspect of the ER fluids with a view to their practical application is related to the leak current between electrodes. The electric field dependence of the leak current density, J(E), is presented in Figure 8 for all the dispersions studied. Cloisite 15A presented a fairly good linear relationship between these two variables, thus obeying the Ohm's law, V = I·R, in the entire E-field range considered, i.e., up to 4 kV/mm (Figure 8b). An increase in the J(E) slope was observed with concentration, as corresponds to the evolution of σ_{AC} plateau value with concentration in Figure 4b. Regarding the nanocelluloses, the above linear relationship only remained up to 2.4 kV/mm. Thus, their overall behavior is better described by a power-law relationship, $J \propto E^n$ [29]. Surprisingly, the measured leak current decreased with increasing concentration (Figure 8a). A possible explanation may be the coupling of side branches (which do not span the electrodes) to the main chains, thus yielding structures which dissipate more energy into the oil bulk. In any case,

the nanocelluloses have demonstrated low energy consumptions. Finally, the halloysite nanotubes presented a nearly constant and extremely low value of J within the entire E-field range studied, even slightly lower than that for neat castor oil, a result which corroborates the AC conductivity behavior in Figure 4b.
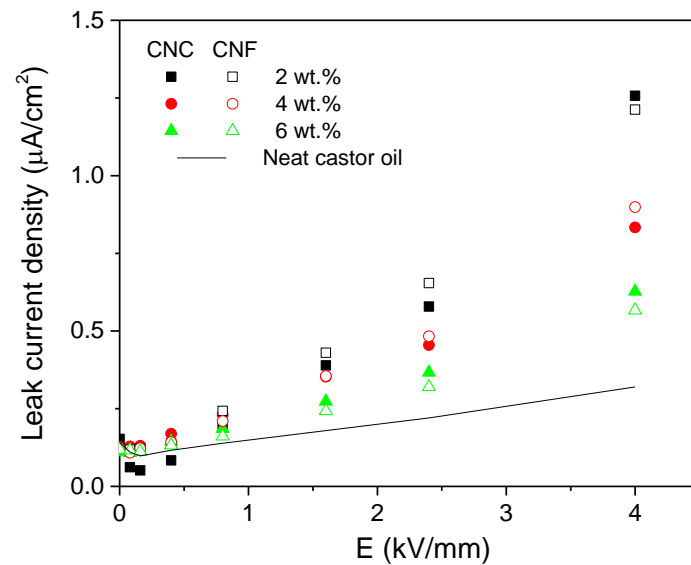
(**a**)
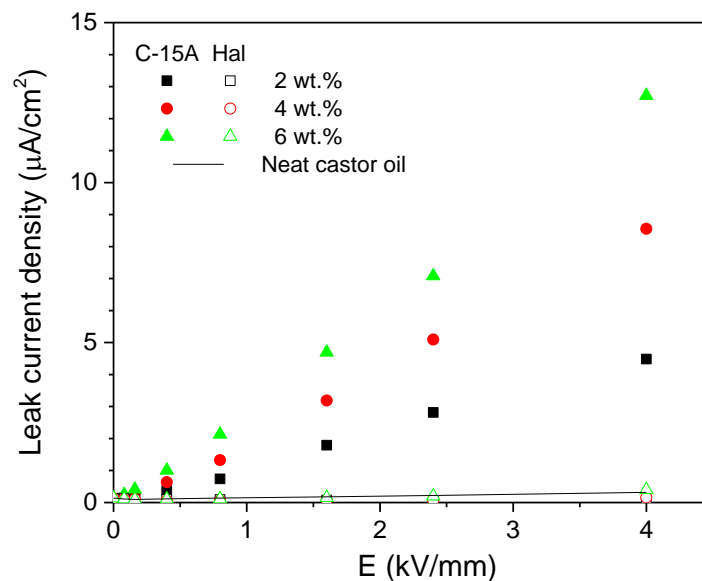
(**b**)

Figure 8. Electric field dependence of the leak current density for (**a**) the nanocelluloses and (**b**) the nanoclays dispersions in castor oil (neat castor oil included for the sake of comparison).

4. Conclusions

The electro-responsive characteristics of cellulose nanocrystals/nanofibrils and Cloisite 15A layered nanosilicate/clay nanotubes in castor oil, at concentrations between 2 and 6 wt.%, were investigated. A preliminary dielectric characterization demonstrated that the nanocelluloses and Cloisite 15A exhibited interfacial polarization under electric fields, within the frequency window of interest for electro-rheology, i.e., 100 Hz to 100 kHz. Moreover, good ER performances were expected in both

cases as deduced from their large values of the permittivity drop $\Delta\varepsilon'$. On the contrary, the halloysite nanotubes, which proved to have a poor polarization capacity, did not show any evidence that interfacial polarization had occurred. The evolution of the static/dynamic yield stress (from viscous flow curves at 25 °C) with the electric field intensity corroborated the previous dielectric results, with values of the yield stress that increased in more than three orders of magnitude with the application of 4 kV/mm in the case of nanocelluloses and Cloisite 15A. This evolution obeyed a power-law scaling, with Cloisite 15A showing larger values of the b exponent than the nanocelluloses, and very close to the theoretical value corresponding to the polarization model, i.e., b = 2. Despite their different aspect ratio, both cellulose nanocrystals and nanofibrils presented very similar behaviors, approaching a limiting yielding behavior as the concentration was increased beyond 4 wt.%, and a critical value of the electric field E_c = 0.94 kV/mm, at 2 wt.%, upon which the b exponent dramatically decreased. Moreover, the nanocelluloses presented a very good balance of high ER response and low leak current values, thus becoming a promising candidate for further studies on the electro-active control of the friction behavior. Despite the higher leak currents exhibited by the Cloisite 15A layered nanosilicate, its electro-tribological behavior is also worth studying, alone or combined with the nanocellulose, given the benefits and implications that may arise from its planar morphology. The nanotubes, instead, presented a poor limiting yielding behavior (or a maximum) with increasing the electric field up to 4 kV/mm, and show, a priori, much less interest from an electro-tribological perspective.

Author Contributions: Conceptualization, M.G.-M., M.A.D. and M.T.C.; methodology, M.G.-M., M.A.D. and S.D.F.-S.; validation, M.G.-M., M.A.D., S.D.F.-S. and C.R.; formal analysis, M.G.-M., M.A.D., S.D.F.-S. and C.R.; investigation, M.G.-M., M.A.D., S.D.F.-S., C.R. and M.A.O.; resources, M.G.-M., M.A.D. and M.A.O.; writing—original draft preparation, M.G.-M.; writing—review and editing, M.G.-M., M.A.D., C.R., M.T.C. and M.A.O.; visualization, M.G.-M., M.A.D., M.T.C. and M.A.O.; supervision, M.G.-M. and M.A.D.; project administration, M.G.-M. and M.A.D.; funding acquisition, M.G.-M., M.A.D. and C.R. All authors have read and agreed to the published version of the manuscript.

Conflicts of Interest: The authors declare no conflict of interest. The funders had no role in the design of the study; in the collection, analyses, or interpretation of data; in the writing of the manuscript, or in the decision to publish the results.

References

1. Madanhire, I.; Mbohwa, C. Lubricant additive impacts on human health and the environment. In *Mitigating Environmental Impact of Petroleum Lubricants*; Springer International Publishing: Cham, Switzerland, 2016; Chapter 2.

2. Quinchia, L.A.; Delgado, M.A.; Valencia, C.; Franco, J.M.; Gallegos, C. Viscosity modification of high-oleic sunflower oil with polymeric additives for the design of new biolubricant formulations. *Environ. Sci. Technol.* **2009**, *43*, 2060–2065. [CrossRef] [PubMed]

3. Quinchia, L.; Canto, M.; Ángel, D.; Reddyhoff, T.; Gallegos, C.; Spikes, H.A. Tribological studies of potential vegetable oil-based lubricants containing environmentally friendly viscosity modifiers. *Tribol. Int.* **2014**, *69*, 110–117. [CrossRef]

4. Delgado, M.; Quinchia, L.; Spikes, H.; Gallegos, C. Suitability of ethyl cellulose as multifunctional additive for blends of vegetable oil-based lubricants. *J. Clean. Prod.* **2017**, *151*, 1–9. [CrossRef]

5. Sánchez, R.; Stringari, G.; Franco, J.M.; Valencia, C.; Gallegos, C. Use of chitin, chitosan and acylated derivatives as thickener agents of vegetable oils for bio-lubricant applications. *Carbohydr. Polym.* **2011**, *85*, 705–714. [CrossRef]

6. Tomala, A.; Kumar, V.B.; Porat, Z.; Michalczewski, R.; Gedanken, A. Tribological anti-wear and extreme-pressure performance of multifunctional metal and nonmetal doped C-based nanodots. *Lubricants* **2019**, *7*, 36. [CrossRef]

7.　Lee, K.; Hwang, Y.; Cheong, S.; Choi, Y.; Kwon, L.; Lee, J.; Kim, S.H. Understanding the role of nanoparticles in nano-oil lubrication. *Tribol. Lett.* **2009**, *35*, 127–131. [CrossRef]

8.　Zhang, Y.; Wei, L.; Hu, H.; Zhao, Z.; Huang, Z.; Huang, A.; Shen, F.; Liang, J.; Qin, Y. Tribological properties of nano cellulose fatty acid esters as ecofriendly and effective lubricant additives. *Cellulose* **2018**, *25*, 3091–3103. [CrossRef]

9.　Martín-Alfonso, J.E.; Martín-Alfonso, M.J.; Franco, J.M. Tunable rheological-tribological performance of "green" gel-like dispersions based on sepiolite and castor oil for lubricant applications. *Appl. Clay Sci.* **2020**, *192*, 105632. [CrossRef]

10.　Barber, G.C.; Jiang, Q.Y.; Zou, Q.; Carlson, W. Development of a laboratory test device for electrorheological fluids in hydrostatic lubrication. *Tribotest* **2005**, *11*, 185–191. [CrossRef]

11.　Hao, T. Electrorheological fluids. *Adv. Mater.* **2001**, *13*, 1847–1857. [CrossRef]

12.　Kimura, Y.; Nakano, K.; Kato, T.; Morishita, S. Control of friction coefficient by applying electric fields across liquid crystal boundary films. *Wear* **1994**, *175*, 143–149. [CrossRef]

13.　Korenaga, A.; Yoshioka, T.; Mizutani, H.; Kikuchi, K. Elastohydrodynamic lubrication characteristics of electrorheological fluids. In *Tribology Series*; Dowson, D., Ed.; Elsevier BV: Amsterdam, The Netherlands, 1999; Volume 36, pp. 517–522.

14.　Seo, Y.P.; Choi, H.J.; Seo, Y. A simplified model for analyzing the flow behavior of electrorheological fluids containing silica nanoparticle-decorated polyaniline nanofibers. *Soft Matter* **2012**, *8*, 4659–4663. [CrossRef]

15.　Liu, Y.D.; Choi, H.J. Electrorheological fluids: Smart soft matter and characteristics. *Soft Matter* **2012**, *8*, 11961–11978. [CrossRef]

16.　Choi, K.; Gao, C.Y.; Nam, J.-D.; Choi, H.J. Cellulose-based smart fluids under applied electric fields. *Materials* **2017**, *10*, 1060. [CrossRef] [PubMed]

17.　Xu, X.; Liu, F.; Jiang, L.; Zhu, J.Y.; Haagenson, D.; Wiesenborn, D.P. Cellulose nanocrystals vs. cellulose nanofibrils: A comparative study on their microstructures and effects as polymer reinforcing agents. *ACS Appl. Mater. Interfaces* **2013**, *5*, 2999–3009. [CrossRef] [PubMed]

18.　Ramos, M.; Rodriguez, J.M.; Delgado, A.V. Electrorheology of clay particle suspensions. Effects of shape and surface treatment. *Rheol. Acta* **2018**, *57*, 405–413. [CrossRef]

19.　Polanský, R.; Kadlec, P.; Kolská, Z.; Švorčík, V. Influence of dehydration on the dielectric and structural properties of organically modified montmorillonite and halloysite nanotubes. *Appl. Clay Sci.* **2017**, *147*, 19–27. [CrossRef]

20.　Peng, J.; Zhu, K.-Q. Hydrodynamic characteristics of ER Journal Bearings with external electric field imposed on the contractive part. *J. Intell. Mater. Syst. Struct.* **2005**, *16*, 493–499. [CrossRef]

21.　Ikazaki, F.; Kawai, A.; Uchida, K.; Kawakami, T.; Edamura, K.; Sakurai, K.; Anzai, H.; Asako, Y. Mechanisms of electrorheology: The effect of the dielectric property. *J. Phys. D Appl. Phys.* **1998**, *31*, 336–347. [CrossRef]

22.　Quinchia, L.; Delgado, M.; Valencia, C.; Franco, J.M.; Gallegos, C.; Canto, M.; Ángel, D. Viscosity modification of different vegetable oils with EVA copolymer for lubricant applications. *Ind. Crop. Prod.* **2010**, *32*, 607–612. [CrossRef]

23.　Maheswaran, R.; Sunil, J. Effect of nano sized garnet particles dispersion on the viscous behavior of extreme pressure lubricant oil. *J. Mol. Liq.* **2016**, *223*, 643–651. [CrossRef]

24.　Chotpattananont, D.; Sirivat, A.; Jamieson, A.M. Scaling of yield stress of polythiophene suspensions under electric field. *Macromol. Mater. Eng.* **2004**, *289*, 434–441. [CrossRef]

25.　Lee, S.; Kim, Y.K.; Hong, J.-Y.; Jang, J. Electro-response of MoS2 nanosheets-based smart fluid with tailorable electrical conductivity. *ACS Appl. Mater. Interfaces* **2016**, *8*, 24221–24229. [CrossRef]

26.　Kuznetsov, N.; Shevchenko, V.G.; Stolyarova, D.; Ozerin, S.A.; Belousov, S.I.; Chvalun, S. Dielectric properties of modified montmorillonites suspensions in polydimethylsiloxane. *J. Appl. Polym. Sci.* **2018**, *135*. [CrossRef]

27.　Roman, C.; García-Morales, M.; Olariu, M.A.; McNally, T. Effect of selective distribution of MWCNTs on the solid-state rheological and dielectric properties of blends of PMMA and LDPE. *J. Mater. Sci.* **2020**, *55*, 1–15. [CrossRef]

28.　Seo, Y.P.; Choi, H.J.; Seo, Y. Analysis of the flow behavior of electrorheological fluids with the aligned structure reformation. *Polymer* **2011**, *52*, 5695–5698. [CrossRef]

29.　Rozynek, Z.; Knudsen, K.D.; Fossum, J.; Méheust, Y.; Wang, B.; Zhou, M. Electric field induced structuring in clay–oil suspensions: New insights from WAXS, SEM, leak current, dielectric permittivity, and rheometry. *J. Phys. Condens. Matter* **2010**, *22*, 324104. [CrossRef]

30. Kuznetsov, N.; Stolyarova, D.Y.; Belousov, S.I.; Kamyshinsky, R.; Orekhov, A.S.; Vasiliev, A.L.; Chvalun, S.N. Halloysite nanotubes: Prospects in electrorheology. *Express Polym. Lett.* **2018**, *12*, 958–965. [CrossRef]

31. Sheng, P.; Wen, W. Electrorheological fluids: Mechanisms, dynamics, and microfluidics applications. *Annu. Rev. Fluid Mech.* **2012**, *44*, 143–174. [CrossRef]

32. Rozynek, Z.; Zacher, T.; Janek, M.; Caplovicova, M.; Fossum, J. Electric-field-induced structuring and rheological properties of kaolinite and halloysite. *Appl. Clay Sci.* **2013**, *77*, 1–9. [CrossRef]

33. Zhang, K.; Gao, C.Y.; Choi, H.J.; Yin, J.; Zhao, X. Rheological analysis of titanium dioxide nano-whisker based electrorheological fluids. *J. Ind. Eng. Chem.* **2020**, *83*, 285–288. [CrossRef]

34. Cho, M.; Choi, H.J.; Jhon, M. Shear stress analysis of a semiconducting polymer based electrorheological fluid system. *Polymer* **2005**, *46*, 11484–11488. [CrossRef]